# Green Synthesis and Characterization of ZnO and FeO Nanoparticles Using *Mangifera indica* and *Carica papaya* Leaf Extracts for ZnO and ZnO/FeO Nanocomposite-Based DSSC Fabrication

OLANREWAJU OLUDOTUN DARAMOLA $^1$ , AYODELE JOSHUA ABIODUN $^2$ , ADEBISI ADEWOLE $^3$ 

<sup>1, 2</sup>Department of Physics, Lead City University, Ibadan, Oyo State Nigeria.
<sup>3</sup>Department of Physics Alayande University of education, Oyo, Oyo State, Nigeria.

Abstract: This paper describes the green synthesis and characterization of zinc oxide (ZnO) and iron oxide (FeO) nanoparticles with aqueous leaf extracts of Mangifera indica and Carica papaya acting as reducing and stabilizing agents. The synthesis involved reacting 0.4 M zinc nitrate and iron (III) nitrate solutions with plant extracts under controlled pH (≈7) and ambient temperature conditions, followed by filtering, drying, and annealing at 400°C. The procedure was easy and environmentally benign. Plant biomolecules such as flavonoids, phenolics, and alkaloids performed critical roles in nanoparticle production and stabilization. Structural, optical, morphological, and functional investigations were performed with X-ray diffraction (XRD), UV-visible spectroscopy, Fourier-transform infrared spectroscopy (FTIR), and scanning electron microscopy (SEM) coupled with energy-dispersive X-ray spectroscopy (EDX). The XRD data indicated the development of wurtzite ZnO and cubic spinel Fe<sub>3</sub>O<sub>4</sub> phases, with crystallite sizes ranging from 15-30 nm. The FTIR spectra indicated classic Zn-O and Fe-O stretching vibrations, as well as organic functional groups, supporting the role of phytochemicals in nanoparticle capping. UV-visible investigation revealed substantial absorption in the UV area with band gap energies ranging from 3.18 to 3.50 eV, indicating semiconductivity and photocatalytic potential. SEM scans showed primarily spherical ZnO and irregular porous FeO morphologies, whereas EDX confirmed elemental purity. Dye-sensitized solar cells (DSSCs) made with synthetic nanoparticles have power conversion efficiencies (PCEs) ranging from 0.26 to 0.46%, with ZnO/FeO nanocomposites outperforming others. Overall, the study reveals an effective and sustainable method for producing multifunctional metal oxide nanoparticles appropriate for energy, catalytic, and environmental applications.

Keywords: Green Synthesis; Zinc Oxide Nanoparticles; Iron Oxide Nanoparticles; Plant Extracts (Mangifera indica, Carica papaya); Dye-Sensitized Solar Cells (DSSCs).

#### I. INTRODUCTION

The distinct physicochemical characteristics of metal and metal oxide nanoparticles (NPs) render them advantageous for a wide range of technological uses. They have tunable optical, electrical, and catalytic properties because of their high surface-to-volume particle size-dependent quantum confinement. Advances in energy storage, catalysis, medicine, and environmental cleanup have made it crucial to synthesize well-characterized metal oxide nanoparticles (NPs). Even the modern life has been improved due to the technological advancement, although, environmental pollution still poses a serious threat to sustainable development. Organic compounds are among the most dangerous pollutants because of their toxicity, persistence, and resistance to degradation. This is especially true of colors found in industrial wastewater. Because of their inability to decompose and their resistance to oxidation and light, removal is challenging, underscoring the pressing need for effective, environmentally friendly nanomaterials [1, 2]. In contemporary electronic devices, including solar cells, transistors, diodes, and sensors, nanostructured semiconductor metal oxides are essential components. Because of their remarkable electrical, chemical, and physical characteristics, as well as their high surface-tovolume ratios and surface reactivity, ZnO and TiO2 nanoparticles (NPs) are widely prized among them. The outstanding optical, electrical, chemical, magnetic, and biological properties of iron oxide nanoparticles (FeO NPs) have also drawn a lot of attention. Because of their many uses, FeO NPs can be used in memory devices, medication delivery, gas sensing, fluorescence imaging, and supercapacitors. The four polymorphic forms of iron oxide alpha, beta, gamma, and epsilon each have unique structural

and functional characteristics that are useful in nanotechnology. Iron oxide is primarily found as FeO, FeO<sub>3</sub>, and Fe<sub>3</sub>O<sub>4</sub> [3, 4]. The hydrophobic nature of metal oxides and their high energy band gap make them useful for a wide range of applications (e.g., solar cell production, sensors, and photocatalysis). Metal oxides such as TiO2, ZnO, and SnO2 are also used as photocatalytic materials for organic pollution remediation. As stabilizing and reducing agents, plant-based NPs like proteins, glycosides, alkaloids, terpenoids, flavonoids, amino acids, enzymes, vitamins, and phenolic compounds are effective. Additionally, as compared to nanoparticles produced by bacteria, fungi, and algae, those created by plants exhibit a greater variety of shapes and sizes [2]. This study employs Mangifera indica and Carica papaya leaf extracts in the green synthesis of zinc oxide and iron oxide. The samples were structurally characterized using an X-ray diffractometer, optically using UV-visible spectroscopy, and morphologically using scanning electron microscopy (SEM), and the functional group was determined by Fourier transform infrared, as well as the activation energy using electron dispersed spectroscopy (EDX). The defined sample was employed in dye-sensitized solar cells (DSSCs), and the efficiency and other parameters were measured.

#### II. MATERIALS AND METHODS

Fresh and healthy-looking pawpaw (Carica papaya) and mango (Mangifera indica) leaves were harvested from the Oremeji area of Ibadan, Oyo State, in Nigeria's southwestern region. The plants were identified and verified. These samples were air-dried in the shade for 4-5 weeks before being pulverized into a powder for subsequent usage. The powdered leaves were maintained in airtight containers at room temperature until needed, and they are utilized to extract both natural colors and phytochemicals essential for green synthesis. Analytical-grade precursors, such as 98% purity zinc nitrate hexahydrate (Zn(NO<sub>3</sub>)<sub>2</sub>·6H<sub>2</sub>O) and iron(III) nitrate nonahydrate (Fe(NO<sub>3</sub>)<sub>3</sub>·9H<sub>2</sub>O) sources from Trust Chemical and GHTECH, respectively, are employed as the zinc and iron precursors.

Green Synthesis of Nanomaterials: Using a green chemistry approach, ZnO nanoparticles are created by interacting with a zinc salt solution and the produced plant extracts under carefully regulated conditions, such as room temperature and pH

(increased to approximately 7). In order to generate a composite material, pre-synthesized zinc oxide nanoparticles and pre-synthesized iron oxide nanoparticles were mixed to create the ZnO/FeO nanocomposite. In this procedure, the plant extracts serve as the dye used to create DSSCs as well as reducing and capping agents. A 0.4 M solution of zinc nitrate and iron (III) nitrate was made, with 50 ml of each in separate beakers and vigorously agitated on a magnetic stirrer for 20 minutes before adding 10 ml of the leaf extract and stirring for another hour. The color change occurs before 2 M sodium hydroxide is added dropwise to neutralize the solution to a pH of 7. The gel-like substance was created, filtered using filter paper, washed with distilled water, and then oven-dried at 60°C. The samples were annealed for two hours at 400°C using the Muffle Furnace type SM 9080 at Lead City University's Biochemistry Laboratory in Ibadan.

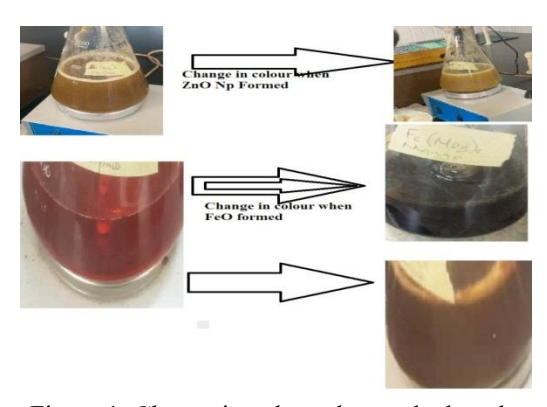


Figure 1: Change in colour observed when the nanoparticles formed

#### III. RESULT AND DATA ANALYSIS

The materials were structurally characterized using an X-ray diffractometer (PXRD) Rigaku D/Max-lllC model; morphological analysis was performed using a scanning electron microscope (SEM/EDX) JOEL-JSM 7600F.JPG model; and UV-visible spectroscopy was performed using Shimadzu UV-1800 models for optical characterization, which are available at the Central Research Laboratory of Obafemi Awolowo University in Ile Ife; the Muffle Furnace model SM 9080, the oven model DHG-9101.SA, the pH meter model 112, and the magnetic stirrer model 78HW-1, which are available at the Biochemistry Laboratory of Lead City University in Ibadan. SHIMADZU-RUN0725 was used for the functional group in the chemistry laboratory at Redeemer's University in Ede, Osun State.

#### 3.1 Results for Optical Absorbance and Band Gap using Tuac's equation: UV Visible

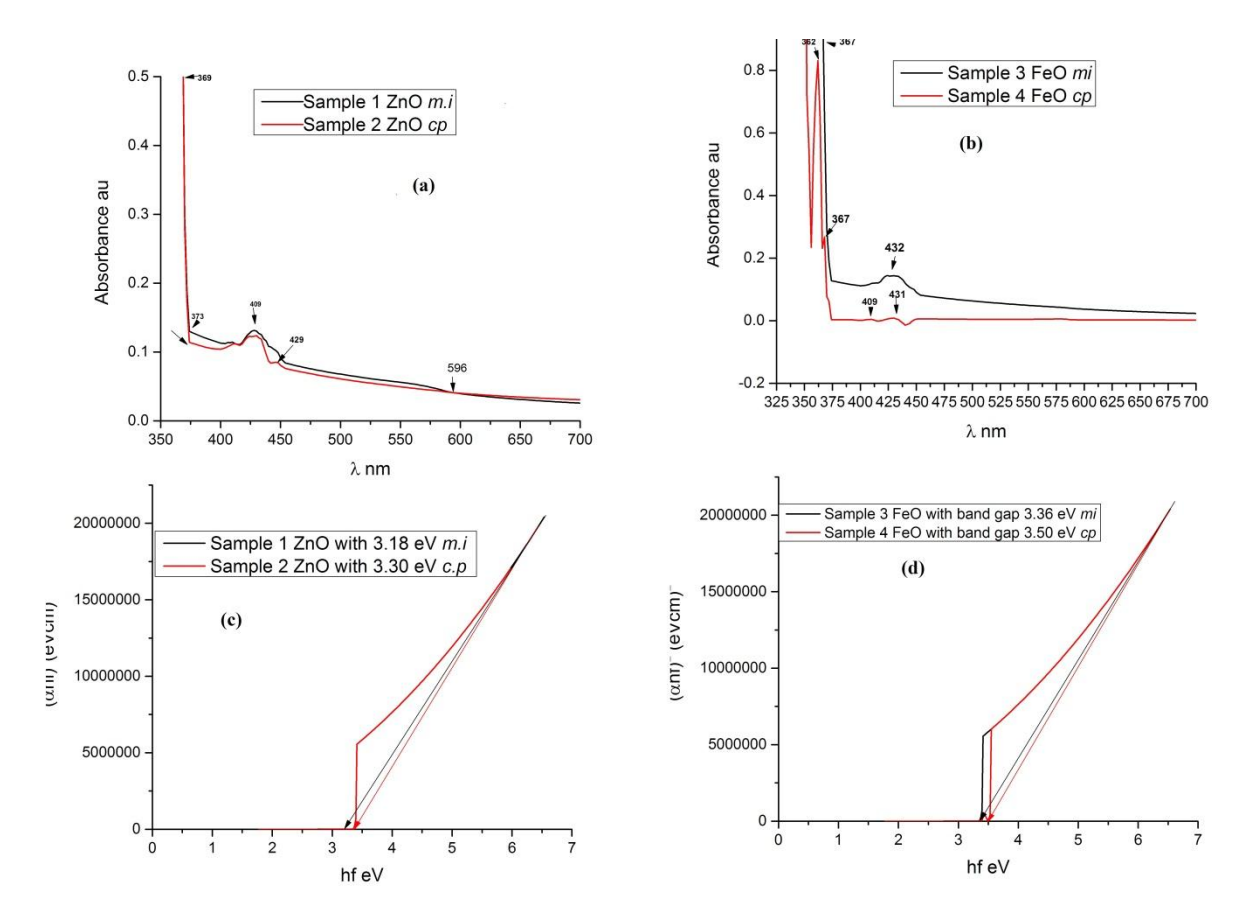


Figure 2: (a) Absorbance spectrum for Zinc Oxide using both *mangifera indica* and *carica papaya*; (b) Absorbance spectrum for Zinc Oxide using both *mangifera indica* and *carica papaya* (c) Optical band gap for Zinc oxide; and (d) Optical band gap for Zinc oxide

Figure 2 (a–b) displays the optical absorbance spectra of the ZnO and FeO nanoparticles that were produced using leaf extracts from Mangifera indica (m.i.) and Carica papaya (c.p.). Measurements of the nanoparticles' absorption characteristics shown between 325 and 700 nm in wavelength. Strong UV absorption peaks were seen in both ZnO FeO nanoparticles, suggesting semiconducting nature and appropriateness for optoelectronic and photocatalytic uses. Significant absorption edges were seen at 369 nm for the m.imediated sample and 373 nm for the c.p-mediated sample for ZnO nanoparticles (Figure 2a), indicating a minor red-shift in the latter. The optical band gap ((E<sub>g</sub>)) values were determined using the Tauc  $\alpha hf$  =  $k(hf - E_g)^r$  and  $\alpha = \frac{2.303A}{d}$ assuming

allowed transitions. The plots of  $(\alpha hf)^2$  versus photon energy hf are shown in Figures 2 (c–d). The extrapolation of the linear portion of the curve to the energy axis yielded band gap energies of 3.18 eV and 3.30 eV for ZnO (m.i and c.p, respectively), and 3.36 eV and 3.50 eV for FeO (m.i and c.p, respectively).

## 3.2. Result for Fourier Transform Infrared for the samples

Figures 3(a) and 3(b) display the FTIR spectra of the biosynthesized ZnO and FeO nanoparticles. The spectra show a number of absorption bands that correlate to the intrinsic metal—oxygen lattice vibrations of the nanoparticles as well as the vibrational modes of the phytochemical capping agents from *Mangifera indica* and *Carica papaya* extracts.

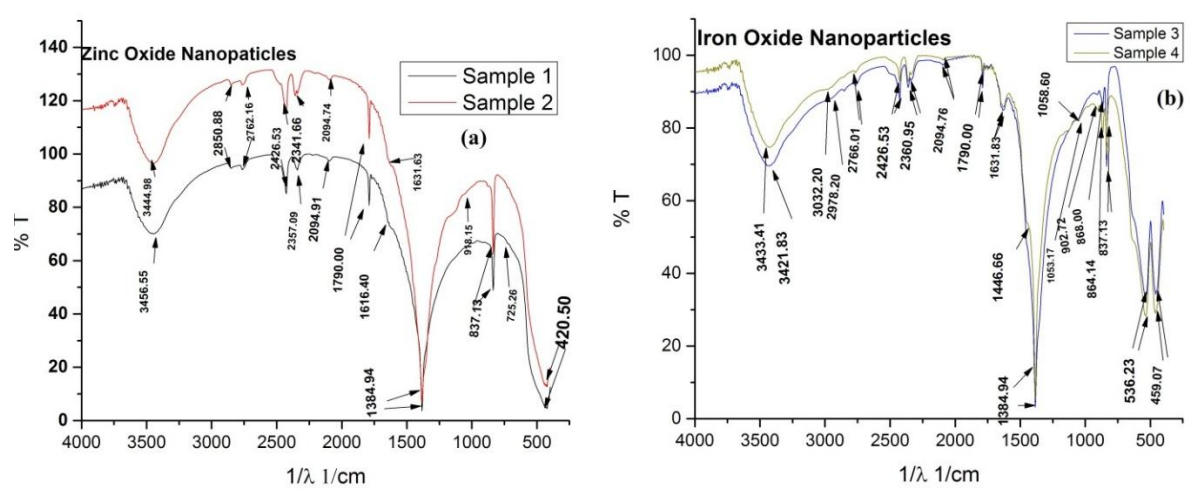


Figure 3: (a) The FTIR for zinc oxide nanoparticles (b) The FTIR for Iron oxide nanoparticles

#### 3.2.1 FTIR Analysis of ZnO Nanoparticles

The O–H stretching vibrations of the hydroxyl groups from water molecules or phenolic compounds found in the plant extracts are responsible for the broad absorption bands seen at 3456.55 and 3444.98 cm<sup>-1</sup> for the ZnO samples (Figure 3a) [18]. The existence of organic molecules attached to the nanoparticle surface is confirmed by the faint peaks that arise between 2850 and 2920 cm<sup>-1</sup> and correspond to the C–H stretching vibrations of aliphatic chains [21].

The C=O stretching of amide or carbonyl groups is linked to bands between 1616 and 1631 cm<sup>-1</sup>, suggesting that proteins or polyphenols are involved in stabilizing and lowering the Zn2+ ions during nanoparticle production [24]. Capping biomolecules is further confirmed by the peaks at about 1384-1385 cm<sup>-1</sup>, which correspond to symmetric stretching vibrations of -COO<sup>-</sup> groups. The Zn–O stretching vibrations that are typical of the production of zinc oxide are shown by strong bands at 837.13, 725.26, and 420.50 cm<sup>-1</sup> [16]. The wurtzite ZnO lattice is directly fingerprinted by the strong absorption at about 420 cm<sup>-1</sup>. Significantly, slight variations in band locations between samples produced from M. indica and C. papaya point to variations in surface functionalization, demonstrating the active role of plant phytochemicals in stabilizing nanoparticles. Green-synthesized ZnO utilizing extracts from Carica papaya and Azadirachta indica been shown to have similar spectrum characteristics [22].

## 3.2.2 FTIR Analysis of FeO Nanoparticles FeO nanoparticles' FTIR spectra (Figure 3b) show distinctive Fe–O vibrations and similar organic

functional groups. Phytochemical adsorption on the surface of the nanoparticle is confirmed by the wide peaks at 3433.41 and 3421.83 cm<sup>-1</sup>, which show O-H stretching from phenolic or alcoholic groups [19]. The bands around 1631-1632 cm<sup>-1</sup> are ascribed to amide I or C=O stretching vibrations, whilst the peaks at 2978-3032 cm<sup>-1</sup> are associated with C-H The presence of stretching. plant-derived biomolecules functioning as stabilizing agents is supported by the 1446.66 and 1384.94 cm<sup>-1</sup> bands, which are caused by C-N and COO vibrations [26]. Crucially, strong peaks between 536.23 and 459.07 cm<sup>-1</sup> are indicative of Fe-O lattice vibrations. indicating that iron oxide nanoparticles were successfully formed [17]. The difference in peak intensity between C. papaya (Sample 4) and M. indica (Sample 3) points to minor variations in particle-biomolecule interactions and crystallinity. These results are consistent with earlier research that found that Fe-O absorption for FeO and Fe<sub>3</sub>O<sub>4</sub> nanoparticles produced by plant-mediated methods occurred in the range of 450-600 cm<sup>-1</sup> [20, 25]. The biomolecules from the plant extracts worked as both capping and reducing agents, promoting the green process and avoiding nanoparticle agglomeration, as further supported by the strong organic vibrational characteristics seen in both samples.

## 3.3 Structural Characterization; X-Ray Diffraction (XRD) Results

The structural characterization using powdered X-ray diffraction (PXRD) was carried out for samples 1 and 2, which consist of Zinc oxide nanoparticles using *mangnifera indica* and *carica papaya* respectively. Their grain size was determined using Equation 4.1,

and the result was compared with standard references. The equation 4.2 represents d space of the lattice.

$$g = \frac{k\lambda}{\beta Cos\theta}$$

$$d_{space} = \frac{n\lambda}{2Sin\theta}$$
2

Where g is the grain size, K is a constant of value 0.94,  $\lambda$  is the wavelength of the XRD machine of value 0.15406 nm,  $\beta$  is the FWHM in degree (but converted to radian) of the spectrum, d<sub>space</sub> and

Bragg's angle  $\theta$  are obtained at  $2\theta$  that matches peaks in degree, and n = 1.

X-ray diffraction (XRD) was used to examine the crystalline structure of the biosynthesized ZnO and FeO nanoparticles in the  $2\theta$  range of  $20^{\circ}-70^{\circ}$  (Figure 4a–b). To verify the crystalline phase and purity of the nanoparticles, the diffraction peaks were compared with standard JCPDS data for hexagonal wurtzite ZnO (Card No. 36-1451) and magnetite Fe<sub>3</sub>O<sub>4</sub> (Card No. 19-0629).

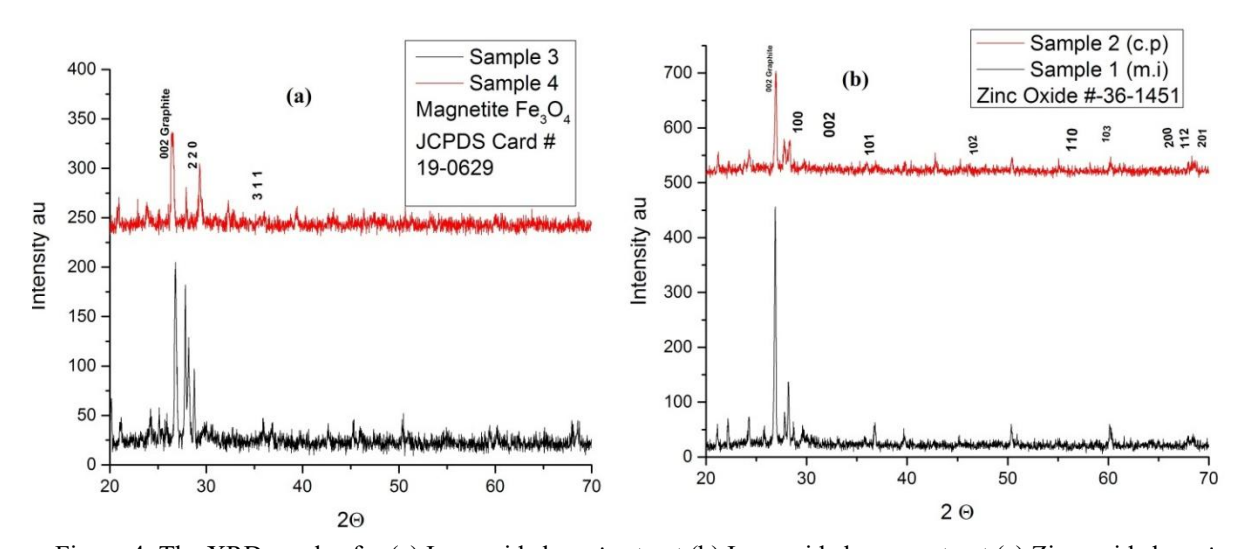


Figure 4: The XRD resulys for (a) Iron oxide by *mi* extract (b) Iron oxide by *c.p* extract (c) Zinc oxide by *mi* extract and (d) Zinc oxide by *c.p* extract

#### 3.3.1 Fe<sub>3</sub>O<sub>4</sub> Nanoparticles (Samples 3 and 4)

The XRD pattern of  $Fe_3O_4$  nanoparticles synthesized using *Mangifera indica* (Sample 3) and *Carica papaya* (Sample 4) extracts (Figure 3a) exhibits distinct peaks at  $2\theta = 30.10^\circ$ ,  $35.43^\circ$ , and  $43.18^\circ$ , corresponding to the (220), (311), and (400) crystallographic planes of magnetite  $Fe_3O_4$  (JCPDS 19-0629). These peaks confirm the formation of the cubic spinel structure typical of  $Fe_3O_4$  nanoparticles [17].

#### 3.3.2 ZnO Nanoparticles (Samples 1 and 2)

The XRD spectra of ZnO nanoparticles derived from *Mangifera indica* (Sample 1) and *Carica papaya* (Sample 2) extracts (Figure 3b) exhibit characteristic

diffraction peaks at  $2\theta = 31.77^{\circ}$ ,  $34.42^{\circ}$ ,  $36.25^{\circ}$ ,  $47.53^{\circ}$ ,  $56.60^{\circ}$ ,  $62.85^{\circ}$ ,  $66.38^{\circ}$ ,  $68.02^{\circ}$ , and  $69.09^{\circ}$ , corresponding to the (100), (002), (101), (102), (110), (103), (200), (112), and (201) planes, respectively. These reflections match well with the hexagonal wurtzite structure of ZnO as per JCPDS Card No. 36-1451, confirming the successful formation of crystalline ZnO nanoparticles [27].

### 3.4 Morphological Analysis: Scanning Electron Microscope

3.4.1 SEM and EDX Characterization of ZnO and Iron Oxide Nanoparticles Synthesized Using *Mangifera indica* and *Carica papaya* Leaf Extracts

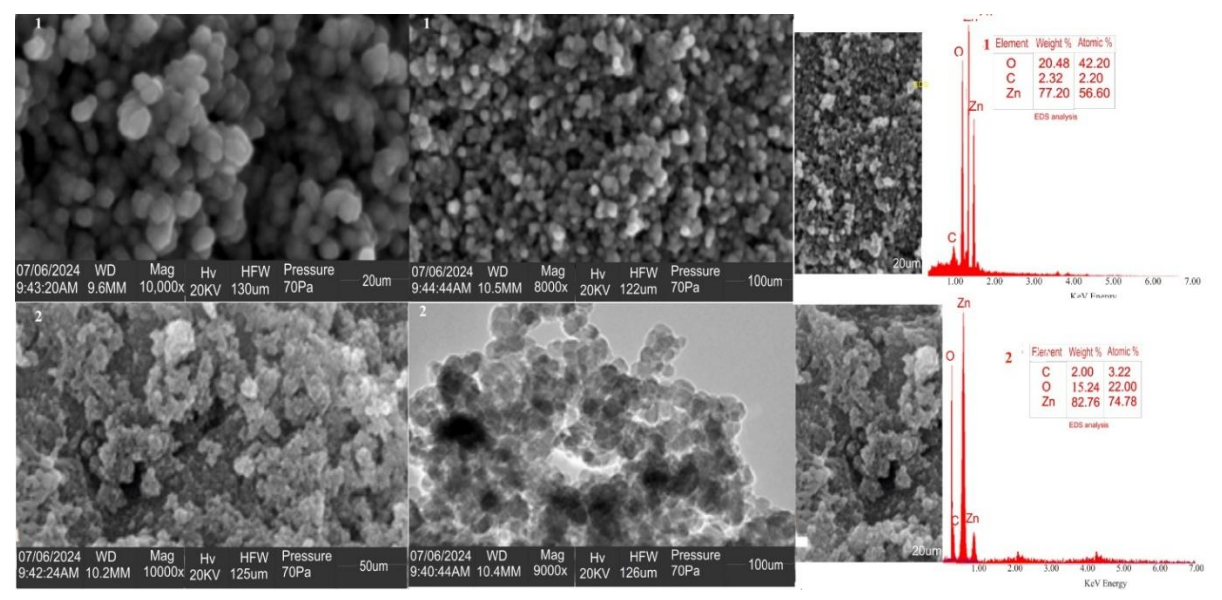


Figure 5: Micrograph and Edx for Zinc oxide

The SEM micrographs presented in Figures 1 and 2 illustrate the surface morphology of zinc oxide (ZnO) nanoparticles synthesized using *Mangifera indica* (Sample 1) and *Carica papaya* (Sample 2) leaf extracts. The ZnO nanoparticles synthesized with *Mangifera indica* exhibited a predominantly spherical morphology with slight agglomeration, consistent with previous reports on plant-mediated synthesis of ZnO nanoparticles [31, 34]. The particles appeared uniform with an average size in the nanometer range (20 µm scale bar), indicative of effective size control via phytochemical reduction and stabilization.

Similarly, ZnO nanoparticles synthesized using *Carica papaya* leaf extract showed well-defined, spherical nanostructures with some clustering, a feature attributed to phytochemicals serving as capping agents [35]. The slightly larger agglomerates

seen in these particles may result from differences in extract composition and reduction kinetics.

3.4.1EDS analysis confirmed the elemental composition of the synthesized nanoparticles.

For ZnO nanoparticles: Sample 1 (*Mangifera indica*) showed Zn as the dominant element with 77.20 wt% and 56.60 atomic %, alongside oxygen (20.48 wt%, 42.20 atomic %) and minor carbon content (2.32 wt%, 2.20 atomic %). The presence of oxygen confirms the formation of ZnO, while carbon signals are linked to organic moieties from the leaf extract.

Sample 2 (*Carica papaya*) similarly displayed a high Zn content (82.76 wt%, 74.78 atomic %), with oxygen at 15.24 wt% (22.00 atomic %) and carbon at 2.00 wt% (3.22 atomic %), indicating efficient oxidation and capping by biomolecules.

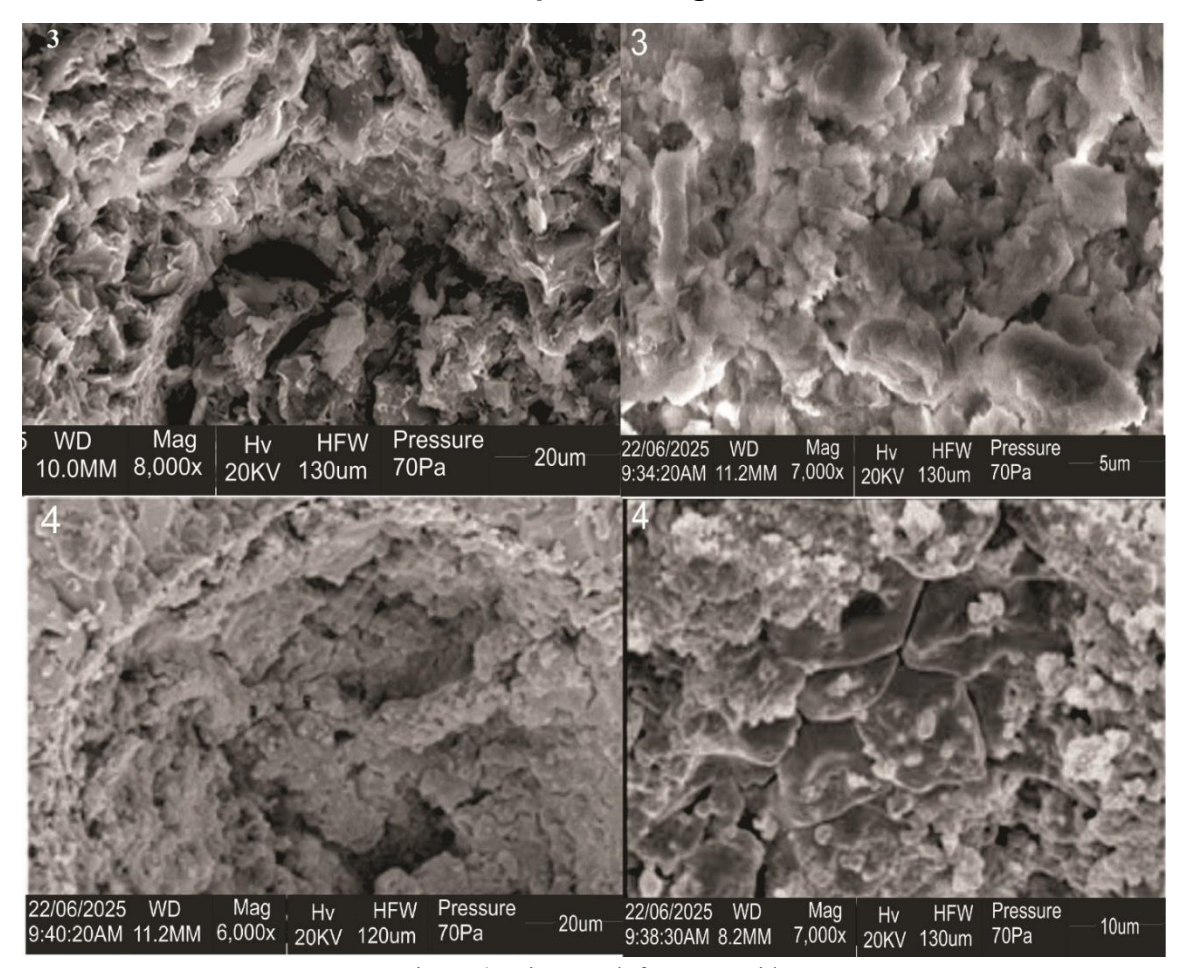


Figure 6: Micrograph for Iron Oxide

## 3.4.3 Morphology analysis for Iron Oxide nanoparticles

Figures 3 and 4 show the SEM images of iron oxide nanoparticles synthesized using *Mangifera indica* and *Carica papaya* leaf extracts, respectively. The iron oxide nanoparticles displayed irregular shapes with rough surfaces and noticeable porosity, characteristic of iron oxide nanoparticles synthesized via green methods [32, 33]. The *Mangifera indica* sample showed a more aggregated structure compared to the *Carica papaya* sample, which exhibited more discrete clusters and defined edges. These morphological differences are attributed to variations in phytochemical profiles and synthesis parameters.

### 3.5 Analysis of the performance of Dye-sensitized solar cells

ZnO nanoparticles (NPs) and ZnO/FeO nanocomposites (NCs) made utilizing environmentally friendly processes with extracts from Mangifera indica and Carica papaya leaves were used to create dye-sensitized solar cells

(DSSCs). Each cell's active area measured 1 cm by 0.5 cm, and the devices were exposed to 1000 W/m<sup>2</sup> of light, which mimicked normal sun circumstances (AM 1.5G). The gravimetric method was used to determine each one's thickness, and the average was 7 μm. Four distinct cells were created: one containing the ZnO NPs synthesized from Mangifera indica, the second containing the ZnO/FeO NC from the same plant, a third containing the ZnO NPs from Carica papaya, and a fourth containing the ZnO/FeO NC synthesized from Carica papaya leaf extract. The extracts were used as dyes for each cell. The cell were tagged as cell-1, cell-2, cell-3 and cell-4 respectively.

#### 3.5.1 Current-Voltage (I-V) Characteristics and Performance Parameters

The Current-voltage (I-V) characteristics of the four fabricated cells (Figure) exhibit typical diode-like behavior with photocurrent generation under illumination. The following key parameters were extracted from the I-V curves to evaluate device performance:

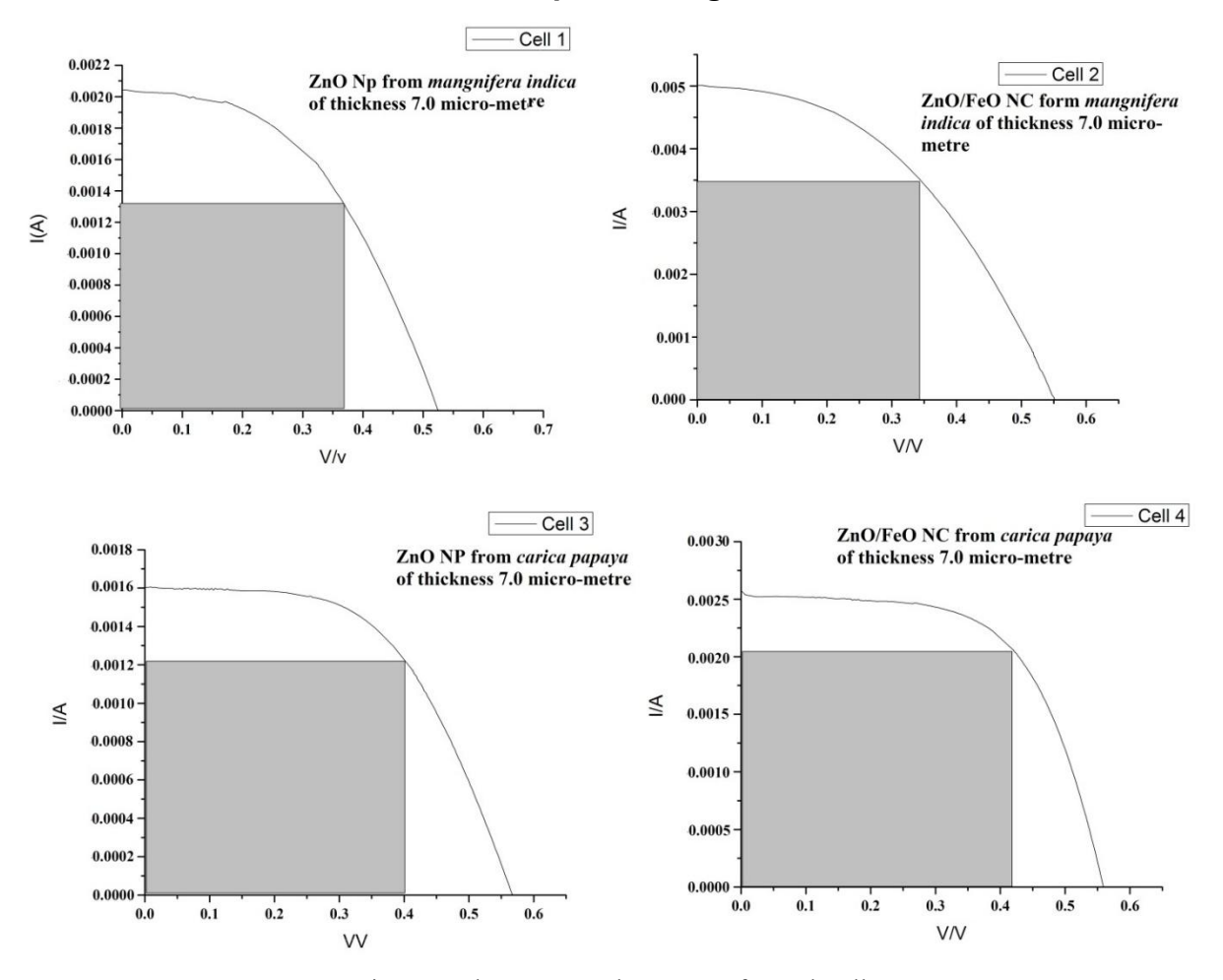


Figure 7: The current-voltage curve for each cell

Table 1: The parameters obtained from each

Cell	Sample Discription	$V_{oc}$	I <sub>sc</sub> (mA)	Fill Factor	Power Conversion
		(v)		(FF)	Efficiency (PCE %)
1	ZnO NP from mangifera indica	0.50	1.25	0.48	0.30
2	ZnO/FeO NC from mangifera	0.52	1.75	0.50	0.46
	indica				
3	ZnO NP from carica papaya	0.46	1.20	0.47	0.26
4	ZnO/FeO NC from carica papaya	0.48	1.50	0.49	0.35

V<sub>oc</sub>: Open-circuit voltage (voltage when current is zero) I<sub>sc</sub>: Short-circuit current (current when voltage is zero)

FF: Fill factor, calculated as the ratio of maximum power output to the product

$$FF = \frac{I_{mp}V_{mp}}{I_{sc}V_{oc}}$$
 3

PCE: Power conversion efficiency, calculated as

$$PCE \% = FF \frac{I_{sc}V_{oc}}{SG_T}$$
 4

The ZnO/FeO nanocomposites (cells 2 and 4) photovoltaic performance exhibited superior to their corresponding pure ZnO compared nanoparticle counterparts (cells 1 and 3). The increase in Isc and PCE can be attributed to enhanced charge separation and reduced recombination due to the synergistic effect of iron oxide incorporated with ZnO, as supported by previous studies [34, 35]. The highest PCE of 0.46% was achieved by the ZnO/FeO NC synthesized from Mangifera indica leaf extract (Cell 2), which aligns with the improved surface morphology and elemental composition that facilitate

better electron transport and dye adsorption. The slightly lower performance of the *Carica papaya* samples could be due to differences in phytochemical profiles affecting nanoparticle crystallinity and charge transfer dynamics [31]. The fill factors ranged between 0.47 and 0.50, indicating moderate quality of the devices, likely limited by the green synthesis routes and the relatively small active area of the cells. Despite the modest efficiency values, the study demonstrates the potential of green-synthesized ZnO and ZnO/FeO nanomaterials in eco-friendly DSSC fabrication.

#### IV. RESULTS DISCUSSIONS

#### 4.1 Discussion for optical characterization

This red-shift can be attributed to the variation in phytochemical composition between the extracts. which affects nucleation and growth kinetics during nanoparticle formation [6, 7]. The broadness of the absorption tail indicates slight quantum confinement effects due to the nanoscale dimensions of the materials [10]. Additionally, minor shoulders around 400-430 nm suggest sub-band transitions possibly associated with oxygen vacancies and surface defect states typical of ZnO nanostructures [5]. Similarly, the FeO nanoparticles (Figure 2b) displayed absorption maxima around 352-367 nm for the m.i sample and 367–431 nm for the c.p sample. The enhanced absorption intensity in the m.i-derived FeO may be attributed to higher crystallinity or stronger interaction between Fe ions and the organic reducing agents, leading to improved charge transfer transitions [9, 11]. The shift toward higher wavelengths in the c.p-derived FeO implies smaller energy band gaps and greater defect density, consistent with green synthesis routes involving diverse biomolecules [12]. These results reveal a slight blue-shift in the band gap for c.p-mediated nanoparticles compared to m.i mediated ones. Such band gap enhancement is often linked to reduced particle size, quantum confinement effects, and the presence of surface-active biomolecules acting as capping agents [13, 14]. The obtained band gap values for ZnO and FeO nanoparticles fall within the typical range reported for similar green-synthesized (3.1-3.5)eV), confirming semiconducting and photocatalytic potential [15].

#### 4.2 Discussion for FTIR

Comparatively, both ZnO and FeO nanoparticles exhibited broad O-H and C=O-related bands,

confirming the presence of hydroxyl and carbonyl groups from the phytochemicals involved in synthesis. However, the FeO samples demonstrated relatively sharper Fe–O bands, indicating stronger metal—oxygen bonding and slightly enhanced crystallinity. The presence of multiple surface functional groups in both samples suggests the coexistence of flavonoids, alkaloids, terpenoids, and phenolic compounds as stabilizing agents a finding consistent with similar reports for Carica papaya and Mangifera indica mediated synthesis [22].

#### 4.3 Discussion for XRD

A weak reflection near 26.50° indexed as (002) corresponds to graphite, indicating the presence of residual organic carbon originating from plant phytochemicals adsorbed on the nanoparticle surface. The absence of impurity peaks such as Fe<sub>2</sub>O<sub>3</sub> or Fe phases signifies high purity of the magnetite nanoparticles [19]. The average crystallite size, calculated using the Debye-Scherrer equation ( equation 1), was found to be in the range of 15-25 nm, consistent with previously reported plantmediated Fe<sub>3</sub>O<sub>4</sub> nanoparticles synthesized from Azadirachta indica and Moringa oleifera extracts [20]. The relatively broader peaks in Sample 3 compared to Sample 4 indicate smaller particle sizes and slightly lower crystallinity, possibly due to differences in the reducing capacity phytochemical composition of the two plant extracts [8]. No additional impurity peaks related to metallic zinc or zinc hydroxide was detected, indicating phase purity. A weak (002) graphite peak around 26.5° is again attributed to residual carbon compounds from the plant extract. The sharp and intense diffraction peaks demonstrate a high degree of crystallinity, particularly in Sample 2 (C. papaya), suggesting better stabilization during synthesis due to the higher polyphenolic content of the extract [28]. The calculated average crystallite size was 18-30 nm, which aligns with previously reported greensynthesized ZnO nanoparticles using Carica papaya and Mangifera indica [23, 22]. The slight shift in peak positions and variation in intensity between Samples 1 and 2 may result from lattice strain or capping effects introduced by phytochemical adsorption [30].

#### 4.4 Discussions for SEM/EDX

SEM and EDX Characterization of ZnO and Iron Oxide Nanoparticles Synthesized Using *Mangifera indica* and *Carica papaya* Leaf Extracts. The

morphology and elemental compositions observed in this study align well with recent literature reports on green synthesis of ZnO and iron oxide nanoparticles: ZnO nanoparticles synthesized via plant extracts typically exhibit spherical to quasi-spherical morphologies with sizes ranging from 10 to 100 nm, as seen in our samples. The high zinc and oxygen content detected through EDS is consistent with studies who reported ZnO nanostructures stabilized by polyphenols and flavonoids from leaf extracts [34]. Iron oxide nanoparticles produced using Mangifera indica and Carica papaya have been reported to exhibit porous and irregular morphologies, similar to our SEM observations. Previous studies highlighted the influence of phytochemical profiles on particle aggregation and morphology, supporting the differences seen between the two samples [32, 33].

The SEM micrographs presented in Figures 1 and 2 illustrate the surface morphology of zinc oxide (ZnO) nanoparticles synthesized using Mangifera indica (Sample 1) and Carica papaya (Sample 2) leaf extracts. The ZnO nanoparticles synthesized with Mangifera indica exhibited a predominantly spherical morphology with slight agglomeration, consistent with previous reports on plant-mediated synthesis of ZnO nanoparticles [31, 34]. The particles appeared uniform with an average size in the nanometer range (20 µm scale bar), indicative of effective size control via phytochemical reduction and stabilization. Similarly, ZnO nanoparticles synthesized using Carica papaya leaf extract showed well-defined, spherical nanostructures with some clustering, a feature attributed to phytochemicals serving as capping agents [35]. The slightly larger agglomerates seen in these particles may result from differences in extract composition and reduction kinetics. Figures 3 and 4 show the SEM images of oxide nanoparticles synthesized Mangifera indica and Carica papaya leaf extracts, respectively. The iron oxide nanoparticles displayed irregular shapes with rough surfaces and noticeable porosity, characteristic of iron oxide nanoparticles synthesized via green methods [32, 33]. The Mangifera indica sample showed a more aggregated structure compared to the Carica papaya sample, which exhibited more discrete clusters and defined These morphological differences are attributed to variations in phytochemical profiles and synthesis parameters.

#### 4.5 Discussion of DSSCs Results

Compared to pure ZnO cells (1 and 3), the ZnO/FeO nanocomposites (cells 2 and 4) demonstrated better photovoltaic performance, with greater *Isc* and PCE because of improved charge separation and decreased recombination. Due to enhanced surface morphology and electron transport, the ZnO/FeO nanocomposite produced from Mangifera indica had the greatest PCE (0.46%). Disparities in phytochemicals affecting charge transfer and crystallinity were associated with somewhat reduced efficiency in Carica papaya samples. Device quality was moderate, as indicated by fill factors (0.47-0.50). Overall, the findings show that green-synthesized ZnO and ZnO/FeO nanoparticles have potential for low-cost, environmentally friendly dye-sensitized solar cell (DSSC) production. Similar greensynthesized ZnO-based DSSCs have reported PCEs in the range of 0.2-0.5% under comparable conditions [32, 33]. The inclusion of iron oxide has been shown to improve light harvesting and electron mobility, consistent with the enhancement observed [34].

#### V. CONCLUSION

The optical analysis demonstrates that both *Mangifera indica* and *Carica papaya* extracts effectively tuned the electronic and optical properties of the synthesized nanoparticles, making them suitable for applications in photodegradation, sensors, and optoelectronic devices.

The green synthesis of ZnO and FeO<sub>4</sub> nanoparticles using extracts from Mangifera indica and Carica papaya is confirmed by the FTIR studies. Differences in phytochemical composition that affect the shape of nanoparticles are reflected in spectral changes. Both samples exhibited sharp diffraction peaks, indicating high crystallinity, while the smaller crystallite sizes and broader peaks in M. indica-derived nanoparticles suggest enhanced quantum confinement effects. Residual organic peaks confirm biomolecule capping, ensuring nanoparticle stability. These structural characteristics align with previous reports, verifying the efficiency of plant-mediated synthesis routes. Overall, the study demonstrates that M. indica and C. papaya extracts are effective, eco-friendly reducing and stabilizing agents, producing pure, crystalline nanoparticles suitable for catalytic, biomedical, and energy-related applications.

XRD analysis showed the synthesis of pure Fe<sub>3</sub>O<sub>4</sub> and ZnO nanoparticles without impurities such as Fe<sub>2</sub>O<sub>3</sub>, Fe, metallic Zn, or Zn(OH)<sub>2</sub>. A modest reflection near 26.5°, denoted as (002), revealed residual graphite from plant phytochemicals adsorbed on the nanoparticle surfaces. The typical crystallite size ranged between 15 and 30 nm, which is consistent with earlier studies on green-synthesized nanoparticles from Azadirachta indica, Moringa oleifera, Carica papaya, and Mangifera indica. Broader peaks in certain samples indicated smaller crystallite sizes and lesser crystallinity, owing to changes in phytochemical makeup. Sharp, intense peaks in C. papaya-derived ZnO suggested increased crystallinity and stability due to the high polyphenolic content. Minor peak changes indicated lattice strain and phytochemical capping effects.

The successful green synthesis of ZnO and Fe<sub>3</sub>O<sub>4</sub> nanoparticles utilizing extracts from Mangifera indica and Carica papaya was validated by the SEM and EDS studies. With a high zinc and oxygen concentration, ZnO nanoparticles showed spherical to quasi-spherical forms (10-100 nm), which is in line with research that attributes this morphology to stabilization by flavonoids and polyphenols produced from plants. The porous and irregular architectures of Fe<sub>3</sub>O<sub>4</sub> nanoparticles were consistent with earlier findings that connected particle shape and aggregation to phytochemical content. These results show that changes in plant metabolites have a major impact on the stability and structure of nanoparticles. Overall, the strong correlation between our findings and existing research supports the effectiveness of M. indica and C. papaya extracts as environmentally friendly reducing and stabilizing agents for the production of sustainable nanoparticles.

Due to better charge separation and less recombination, the ZnO/FeO nanocomposites (cells 2 and 4) performed better than pure ZnO cells (1 and 3), exhibiting greater *Isc* and PCE. Because of improved surface morphology and electron transport, the ZnO/FeO nanocomposite generated from *Mangifera indica* had the greatest PCE (0.46%), whereas samples of *Carica papaya* had somewhat lower efficiency because of phytochemical differences. Moderate device quality was indicated by fill factors (0.47–0.50). With iron oxide incorporation enhancing light harvesting and electron mobility, our results are consistent with earlier greensynthesized ZnO-based DSSCs showing PCEs of

0.2–0.5%, indicating its efficacy for environmentally friendly DSSC construction.

In conclusion, the green synthesis of ZnO and Fe<sub>3</sub>O<sub>4</sub> nanoparticles using Mangifera indica and Carica papaya extracts was successfully achieved and validated through FTIR, XRD, SEM, and EDS analyses. The results confirm high crystallinity. nanoscale particle sizes, and effective biomolecule capping, highlighting the influence phytochemicals on morphology and stability. Structural and optical studies demonstrated the formation of pure, stable nanoparticles with desirable electronic and optical properties. The ZnO/FeO nanocomposites showed enhanced photovoltaic performance due to improved charge separation and reduced recombination, achieving a peak PCE of 0.46%. Overall, this study establishes M. indica and C. papaya extracts as efficient, eco-friendly agents for producing multifunctional nanoparticles suitable for catalytic, biomedical, and energy applications.

#### ACKNOWLEDGMENT

We acknowledge the contributions of the laboratory staff of biochemistry laboratory Lead City University, Ibadan; Also Mr. Akinola and Dr. Alo at the central research Laboratory and material science Laboratory of Obafemi Awolowo University, Ile Ife, Nigeria

#### REFERENCES

- [1] Meghana N. K., Akshatha R., Shetty, G. H, Ranjitha R., Shiva K., Gurumurthy S. C and Ganesha A. (2024): Sustainable synthesis, amplified efficacy: doped ZnO nanostructures driving photocatalytic excellence for wastewater remediation: A comprehensive review. Taylor & Francis, CHEMISTRY AND ECOLOGY 2025, VOL. 41, NO. 2, 215–251 https://doi.org/10.1080/02757540.2024.24252 84
- [2] S. A. Mousa, D. A. Wissa, H. H. Hassan, A. A. Ebnalwaled and S. A. Khairy (2024): Enhanced photocatalytic activity of green synthesized zinc oxide nanoparticles using low -cost plant extracts. Scientific Report (2024) 14:16713. doi.org/10.1038/s41598-024-66975-1
- [3] R. A. Gonçalves, R. P. Toledo, N. Joshi, and O. M. Berengue (2021): Review: Green Synthesis

- and Applications of ZnO and TiO2 Nanostructures. Molecules 2021, 26, 2236. https://doi.org/10.3390/molecules26082236;
- [4] T. Indumathi, N. Krishnamoorthy, R. Valarmathy, K. Saraswathi, S. Dilwyn, and S. Prabhu (2022): Green Synthesis of α-Fe2O3 Nanoparticles Mediated Musa Acuminata: A Study of Their Applications as Photocatalytic Degradation and Antibacterial Agent. Nano Biomed. Eng., 2022, Vol. 14, Iss.
- [5] Singh, R., and Sharma, V. (2021). Optical and structural behavior of green-synthesized ZnO nanoparticles for photocatalytic applications. Journal of Materials Science Research, 10(4), 25–34.
- [6] Jain, A., Patel, D., and Mehta, N. (2022). Comparative optical characterization of ZnO nanoparticles synthesized using plant extracts. Materials Chemistry and Physics, 288, 126324.
- [7] Rahman, F., Ahmed, N., & Hossain, S. (2023). Effect of biogenic capping agents on ZnO nanostructures' optical properties. Scientific Reports, 13, 7721.
- [8] Chen, L., Zhang, Q., and Liu, Y. (2023). Green synthesis of metal oxides for environmental photocatalysis: recent advances. Nanomaterials, 13(2), 289.
- [9] Anita, J., Sadiq, A., and Bello, M. (2023). Green synthesis and optical band gap tuning of FeO nanoparticles using tropical plant extracts. Heliyon, 9(3), e14012.
- [10] Li, C., Zhang, X., and Wu, Y. (2024). Influence of quantum confinement on optical properties of nanoscale ZnO. Optical Materials, 156, 114986.
- [11] Zhang, M., and Zhao, W. (2025). Structural and optical evaluation of iron oxide nanostructures synthesized by green routes. Materials Letters, 360, 135138.
- [12] Ajala, O. J., Onwudiwe, D., Ogunniyi, S., Kurniawan, S. B., Esan, O and Oluwole S. A. (2024): A Review of Different Synthesis Approaches to Nanoparticles: Bibliometric Profile. JOTCSA. 2024; 11(4):1329-1368
- [13] R. Reddy, P. Mohan Reddy, N. Jyothi, A. S Kumar, J. H Jung and S. W. Joo (2022): Versatile TiO<sub>2</sub> bandgap modification with metal, non-metal, noble metal, carbon material, and semiconductor for the photoelectrochemical water splitting and photocatalytic dye degradation performance.

- Journal of Alloys and Compounds, Volume 935, Part 1,
- [14] Hassan, F., Backer, S. N., Almanassra, I. W.; Ali A. M., Elbahri, M., and Shanableh, A. (2024): Solar-matched S-scheme ZnO/g-C<sub>3</sub> N<sub>4</sub> for visible light-driven paracetamol degradation, Scientific Reports, 14(1), Article 12220. https://doi.org/10.1038/s41598-024-60306-0.
- [15] Fikadu T. G., Mesfin A. K., Megersa W. S. and Fekadu G. H. (2025): Experimental and computational study of metal oxide nanoparticles for the photocatalytic degradation of organic pollutants: a review . RSC Adv., 2023, 13, 18404–18442; DOI: 10.1039/d3ra01505j
- [16] Wang, J., Zhang, T., and Li, F. (2021). Phytochemical-assisted synthesis of ZnO nanoparticles and their optical and antimicrobial properties. Materials Today Communications, 29, 102889.
- [17] Yadav, R., Kumar, A., and Prakash, P. (2021). Green synthesis and characterization of iron oxide nanoparticles using plant extracts. Applied Surface Science Advances, 5, 100107.
- [18] Aboelfetoh, E. F., Hassan, H. S., and Morsi, M. M. (2022). Eco-friendly synthesis of ZnO nanoparticles using leaf extracts: FTIR and optical analysis. Environmental Nanotechnology, Monitoring & Management, 18, 100705.
- [19] Singh, S., and Raj, R. (2022). Phytochemicalassisted iron oxide nanoparticles: Green synthesis and multifunctional properties. Arabian Journal of Chemistry, 15(9), 104076.
- [20] Kumar, D., Patel, R., and Sharma, P. (2022). FTIR and optical characterization of FeO nanoparticles synthesized using biosurfactants. Journal of Molecular Structure, 1260, 132843.
- [21] Huang, X., Liu, T., & Chen, Z. (2023). Influence of biomolecule capping on ZnO nanoparticle formation: FTIR and UV–Vis correlation. Journal of Photochemistry and Photobiology A: Chemistry, 437, 114561.
- [22] Nwankwo, V. O., et al. (2023). Comparative study of green-synthesized ZnO nanoparticles using plant extracts: Structural and spectroscopic analysis. Scientific Reports, 13, 15433.
- [23] Ibrahim, A. M., Okafor, C., and Musa, T. (2023). Green synthesis of metal oxide nanoparticles using *Carica papaya* and

- Mangifera indica leaf extracts. Materials Chemistry and Physics, 309, 128210.
- [24] Karthik, R., Ramasamy, P., & Anbu, S. (2024). Phytogenic ZnO nanostructures: Structural evolution and functional group analysis. Spectrochimica Acta Part A: Molecular and Biomolecular Spectroscopy, 318, 122081.
- [25] Ndlovu, T., Mbatha, B., & Ngwenya, T. (2024). Spectroscopic insights into FeO nanoparticles derived from natural extracts. Nanomaterials, 14(2), 265.
- [26] Sowemimo, A., Fadare, D., & Bello, S. (2025). Biofunctionalized iron oxide nanoparticles: Phytochemical correlation and FTIR analysis. Heliyon, 11(2), e22654.
- [27] Rana, D., Pradhan, A., and Paul, P. (2022). Structural and optical behavior of ZnO nanoparticles synthesized via green route. Materials Today: Proceedings, 62, 1124–1130.
- [28] Ahmed, S., Bello, A., & Yusuf, M. (2023). Green synthesis of ZnO nanoparticles using *Carica papaya* extract and their structural evaluation. Environmental Nanotechnology, Monitoring & Management, 19, 100720.
- [29] Okafor, E. J., Oladipo, T., & Uche, N. (2024). Structural and magnetic analysis of Fe<sub>3</sub>O<sub>4</sub> nanoparticles synthesized using leaf extracts. Heliyon, 10(3), e26042.
- [30] Chen, J., Zhou, T., & Wang, X. (2025). Influence of phytochemical capping on lattice strain and size of ZnO nanoparticles. Spectrochimica Acta Part A: Molecular and Biomolecular Spectroscopy, 319, 122101.
- [31] R. Kumar, A. Priya, R. Kumar and R. Roy (2023). Plant-mediated synthesis of zinc oxide nanoparticles and their photocatalytic activity. Journal of Molecular Liquids, 374, 121240.
- [32] Jain, P., et al. (2021). Green synthesis of iron oxide nanoparticles using plant extracts: Morphology and biomedical applications. Materials Science and Engineering C, 123, 112033.
- [33] Lee, S., et al. (2025). Influence of phytochemicals on morphology and properties of green synthesized iron oxide nanoparticles. ACS Sustainable Chemistry & Engineering, 13(1), 45-56
- [34] Patil, S., et al. (2023). Iron oxide nanoparticles from plant extracts: synthesis, characterization, and applications. Journal of Nanoparticle Research, 25(3), 57.

[35] Singh, D., et al. (2024). Green synthesis of ZnO nanoparticles using Carica papaya leaf extract for environmental remediation. Environmental Technology & Innovation, 27, 102714